Materials Advances

ROYAL SOCIETY OF CHEMISTRY

PAPER

View Article Online
View Journal

Cite this: DOI: 10.1039/d5ma01242b

High performance mercury sensing enabled by the synergistic effect of rGO–MnO_2 nanocomposites

Md Emon Hasan Sourav,[a] Md Tawabur Rahman, *[a] Md Nazmul Islam,[a] Mohammad Abu Yousuf, *[b] Parbhej Ahamed,[b] Habiba Jahan[b] and Nusrat Tazeen Tonu [b]

Access to safe and clean water remains a major global concern, largely due to contamination by toxic heavy metals. Among these contaminants, mercury exhibits extreme toxicity even at ultra-trace level concentrations, posing serious and long-lasting threats to both human health and the environment. To mitigate this issue, a highly selective and sensitive electrochemical sensor has been fabricated for Hg^{2+} ion detection at the trace level. The sensor is designed on a glassy carbon electrode (GCE), which has been modified with a nanocomposite composed of manganese dioxide (MnO_2) nanoparticles and reduced graphene oxide (rGO). Incorporation of rGO and MnO_2 nanoparticles improves electrical conductivity, enlarges the electroactive surface area, and provides abundant adsorption sites for Hg^{2+} ions. MnO_2 serves as a redox-active component with strong affinity for mercury ions (Hg^{2+}), whereas rGO ensures efficient electron transfer. The combined effects of these materials result in a synergistic interface exhibiting excellent electrocatalytic activity, enabling ultrahigh sensitivity, broad detection capability, and a remarkably low detection limit of 0.097 nM – well below the World Health Organization's permissible concentration for Hg^{2+} in drinking water. Furthermore, the developed sensor exhibits long-term operational stability, reproducibility, and repeatability, along with strong selectivity against common interfering ions such as Na^{+}, K^{+}, Fe^{3+}, Zn^{2+}, and Cu^{2+}.Overall, the rGO–MnO_2 nanocomposite modified sensor offers a reliable, cost-effective, and efficient approach for real-time detection and monitoring of Hg^{2+} contamination in aqueous systems.

Received 28th October 2025,
Accepted 22nd April 2026

DOI: 10.1039/d5ma01242b

rsc.li/materials-advances

1. Introduction

The persistence and extreme toxicity of heavy metals remain a major challenge for environmental monitoring and management.[1] Among these pollutants, mercury ions (Hg^{2+}) are regarded as particularly dangerous, even at ultra-trace concentrations because of their strong bioaccumulation and toxic interactions with living systems.[2] Maximum allowable concentrations of Hg^{2+} in drinking water have been set at 5 nM by the United States Environmental Protection Agency (US EPA) and 10 nM by the World Health Organization (WHO).[3] Atmospheric deposition, rock weathering, agricultural runoff, and industrial activities represent major natural and human-driven sources of Hg^{2+} contamination in aquatic systems. Prolonged exposure to Hg^{2+} has been linked to adverse effects on the kidneys, brain, nervous system, immune system, and endocrine functions in both humans and wildlife.[4] Therefore, early and precise detection of Hg^{2+} ions in water resources is essential for ensuring environmental and public health safety.

Traditional analytical approaches for detecting metal ions – including surface-enhanced Raman scattering, inductively coupled plasma mass spectrometry, fluorescence-based assays, and atomic absorption spectroscopy – provide high sensitivity and accuracy for metal ion detection.[5,6] However, their reliance on sophisticated instrumentation, trained personnel, and controlled laboratory settings makes them unsuitable for routine or in-field analysis.[7] In comparison, electrochemical sensors offer a more accessible and efficient alternative. They are cost-effective, easy to use, portable, and capable of delivering real-time results – making them highly suitable for environmental field applications.[8]

Reduced graphene oxide (rGO) has attracted significant interest as a sensing material owing to its exceptional electrical conductivity, chemical stability, and large surface area, which together facilitate efficient detection of trace metal ions such as Hg^{2+}.[9] Its large surface area enhances analyte adsorption, while

[a] Department of Electrical and Electronic Engineering, Khulna University of Engineering & Technology, Khulna 9203, Bangladesh. E-mail: tawabur@eee.kuet.ac.bd
[b] Department of Chemistry, Khulna University of Engineering & Technology, Khulna 9203, Bangladesh. E-mail: yousuf@chem.kuet.ac.bd

its excellent conductivity facilitates rapid electron transfer, making it a promising platform for electrochemical sensor development.[10] However, rGO alone exhibits limited intrinsic redox activity and selectivity toward specific heavy metal ions.[11] To mitigate these limitations, rGO is commonly coupled with redox-active functional materials. Manganese dioxide (MnO_2) is one such effective material.[12] Previous research has shown that Mn-based oxides can be successfully integrated with carbon nanostructures for various composites.[13] Nevertheless, the poor electrical conductivity of MnO_2 restricts its use as a standalone electrode modifier in advanced sensor designs.[14] Therefore, the combination of MnO_2 with conductive rGO has shown great potential. The combination of these two materials in a composite combines the superior conductivity and mechanical robustness of rGO with the adsorption and redox properties of MnO_2.[12] Pathak *et al.* developed Fe_3O_4–MnO_2@rGO nanocomposites and observed enhanced adsorption and catalytic performance for environmental cleanup and sensing tasks.[15] For hydrazine sensing, a hydrothermally synthesized α-MnO_2/N-rGO composite showed improved electrochemical activity and stability.[16] The unique combination of rGO–MnO_2 in nanocomposites offers excellent improvement in electrochemical performance. Yet, their use in detecting Hg^{2+} has received little attention so far. For example, Mnyipika *et al.* developed an MnO_2@rGO nanocomposite-based electrochemical sensor for detecting Cd^{2+}, Zn^{2+}, and Cu^{2+} at the same time, highlighting its promise for multiplexed sensing applications.[17] Several nanostructures, such as silver nanowires, gold nanoparticles, and graphene quantum dots, have also been employed to enhance sensor performance for Hg^{2+} detection. For instance, Rahman *et al.* developed a graphene oxide–silver nanowire (GO–AgNW) composite-based Hg^{2+} sensor with high sensitivity and a low detection limit of ~0.1 nM.[18] Similarly, quantum dot-based sensors like GQDs–AuNPs/GCE have demonstrated excellent performance toward Hg^{2+} with a low detection limit of 0.02 nM.[19] However, these materials are often expensive, involve complex fabrication steps, or may lack long-term environmental stability, issues that limit their practical deployment.

In this work, we emphasize the development and optimization of a cost-effective sensor capable of detecting ultra-trace levels of Hg^{2+} ions in aqueous solution. The rGO–MnO_2 nanocomposite-modified GCE has been fabricated using the solution-mixing technique. The resulting rGO–MnO_2 sensor showed excellent sensing properties toward Hg^{2+} detection even at low concentrations. Furthermore, excellent selectivity was achieved toward Hg^{2+} compared to other metal ions including Na^+, K^+, Zn^{2+}, Fe^{3+}, and Cu^{2+}. Additionally, the sensor showed good reproducibility, repeatability, and stability for the detection of Hg^{2+}.

2. Experimental section

2.1. Materials

All chemicals and reagents used in this work were of analytical grade and were utilized exactly as received, without any further purification steps. Potassium ferricyanide ($K_3[Fe(CN)_6]$) and potassium dihydrogen phosphate (KH_2PO_4) were procured from Sigma-Aldrich (USA). Additionally, rGO was also acquired from Sigma-Aldrich (USA). MnO_2 was prepared and characerized in our laboratory. Ionic solutions for selectivity and interference studies were prepared using a variety of metal salt standards such as lead(II) chloride ($PbCl_2$), copper(II) chloride ($CuCl_2$), iron(III) chloride ($FeCl_3$), sodium chloride (NaCl), potassium chloride (KCl), and mercury(II) chloride ($HgCl_2$), all acquired from Thermo Fisher Scientific (USA). A buffer solution of 0.1 M KH_2PO_4 with a pH of approximately 7.3 was prepared and functioned as the supporting electrolyte in all electrochemical measurements. For cyclic voltammetry (CV) and electrochemical impedance spectroscopy (EIS), a standard redox solution containing 5.0 mM $K_3[Fe(CN)_6]$ dissolved in 0.1 M KCl was prepared to maintain consistent ionic conductivity.

2.2. Instrumentation and characterization techniques

A BioLogic SP-300 potentiostat/galvanostat (Japan) was used for all electrochemical measurements, using a typical three-electrode electrochemical cell. This setup consisted of a 3 mm diameter GCE as the working electrode, while a platinum (Pt) wire functioned as the counter electrode, and an Ag/AgCl (saturated KCl) electrode was used as the reference electrode. The geometric active surface area of the GCE was about 0.227 cm^2. CV and EIS were used to characterize the electrochemical properties of the sensor, whereas square wave anodic stripping voltammetry (SWASV) was applied to identify the Hg^{2+} ions in the samples. Structural features of the synthesized rGO–MnO_2 nanocomposite were analyzed by benchtop X-ray diffraction (XRD) (Bruker D2 PHASER, Germany). Field emission scanning electron microscopy (FESEM) (JEOL JSM-7610F, Japan) was used to analyze the characteristics of rGO–MnO_2. Energy-dispersive X-ray spectroscopy (EDS) coupled with the FESEM system was used to further establish the distribution and composition of the elements in the composite material. Fourier transform infrared spectroscopy (FTIR) (Shimadzu IRTracer-100, Japan) was carried out to further investigate the interaction between Hg^{2+} and the rGO–MnO_2 nanocomposite.

2.3. Sensor fabrication

The stepwise fabrication procedure of the rGO–MnO_2 modified GCE is schematically presented in Fig. 1. At first, the bare GCE was polished using a 0.05 μm alumina slurry on a polishing pad to achieve a mirror-like surface. The polished electrode was then rinsed thoroughly with deionized (DI) water to remove residual alumina particles and subsequently sonicated in DI water for approximately 5 minutes to remove surface irregularities and enhance the electroactive surface area. After cleaning, the electrode was subsequently dried under ambient air at room temperature for approximately 30 minutes, prior to modification.

rGO and MnO_2 powders were co-dispersed in ethanol at a mass ratio of 1 : 3, with a total concentration of 1 mg mL^{-1} for the synthesis of the rGO–MnO_2 nanocomposite. The dispersion was then ultrasonicated in a bath sonicator for 60 minutes to achieve homogeneous mixing and effective interfacial

Fig. 1 Schematic of the fabrication process of an rGO–MnO_2 nanocomposite modified GCE electrode.

interaction between the rGO sheets and MnO_2 nanoparticles. The resulting dark brown-black suspension indicates uniform dispersion of the nanomaterials, suitable for electrode modification. A 5–10 μL of the prepared nanocomposite was drop-cast on the electrode surface and allowed to dry under ambient conditions, allowing complete evaporation of the ethanol solvent and the formation of a stable, uniform coating. The rGO–MnO_2 modified electrode was subsequently stored in a desiccator until use in electrochemical measurements.

3. Results and discussion

3.1. Structural and morphological characterization of rGO, MnO_2, and the rGO–MnO_2 nanocomposite

XRD patterns of MnO_2 nanoparticles, rGO, and rGO–MnO_2 nanocomposite are shown in Fig. 2(a).The measurements were made in order to examine the composite material's successful production, phase purity, and crystalline structure. A broad diffraction peak for rGO is observed at about 26°, which corresponds to the (002) crystal plane of rGO.[19] This broad peak reflects the partially disordered structure and turbostratic stacking of graphene layers resulting from the chemical reduction of rGO.[20] The absence of sharp peaks confirms the amorphous or semi-crystalline nature of the rGO and suggests the presence of residual oxygen-containing functional groups.[10] The XRD pattern of MnO_2 nanoparticles shows a series of sharp and well-defined peaks at 2θ values approximately at 12.7°, 18.0°, 28.7°, 37.4°, 49.8°, and 60.2°.[21] These diffraction peaks match well with the standard γ-MnO_2 diffraction pattern, confirming the successful synthesis of crystalline MnO_2 with high structural order.[22] The sharp and intense reflections of the diffraction peaks confirm the good crystallinity and phase purity of the MnO_2 nanoparticles. The XRD pattern of the rGO–MnO_2 nanocomposite shows features of both rGO and MnO_2, though with weakened intensity and broader peaks. Specifically, the (002) peak of rGO is significantly reduced, while the MnO_2 peaks also appear broadened and suppressed.[23] These observations suggest uniform dispersion of MnO_2 nanoparticles on rGO sheets, which disrupts long-range crystalline order. The broadening of diffraction peaks in the composite indicates the formation of a nanostructured hybrid material with smaller grain size and enhanced lattice disorder due to interaction between the two phases.[24] Importantly, no impurity or secondary-phase peaks are observed in the composite spectrum, which confirms the successful formation and high phase purity of the synthesized rGO–MnO_2 nanocomposite. The diminished intensity and broadened shape of the diffraction peaks support the strong interfacial interaction between rGO and MnO_2, which is critical for enhancing the composite's electrochemical properties.

The FESEM images in Fig. 2(b) show rGO sheets that displayed a crumpled and wrinkled morphology, which is typical of thermally or chemically synthesized rGO. This folded structure offers a large surface area with a significant number of defect sites, advantageous for metal ion adsorption. These wrinkled layers result from the removal of oxygen-containing groups during reduction, partially restoring the conjugated graphene structure and causing the sheets to collapse and fold.[25] It also indicates the presence of thin, transparent layers with a high degree of agglomeration, suggesting a large surface area, which is advantageous for electrochemical sensor applications. Such morphology provides abundant active sites and enhances electron transfer, both of which are critical for the highly sensitive and selective identification of Hg^{2+} ions in water. Fig. 2(c) shows the highly aggregated structure of MnO_2. MnO_2 nanoparticles appeared as spherical and aggregated clusters, consistent with γ-MnO_2 morphology.[21] These particles offered numerous electroactive sites for redox interactions and improved the overall electrochemical performance. The magnified image of MnO_2 exhibits spherical shaped morphology, facilitating enhanced electron transfer due to improved

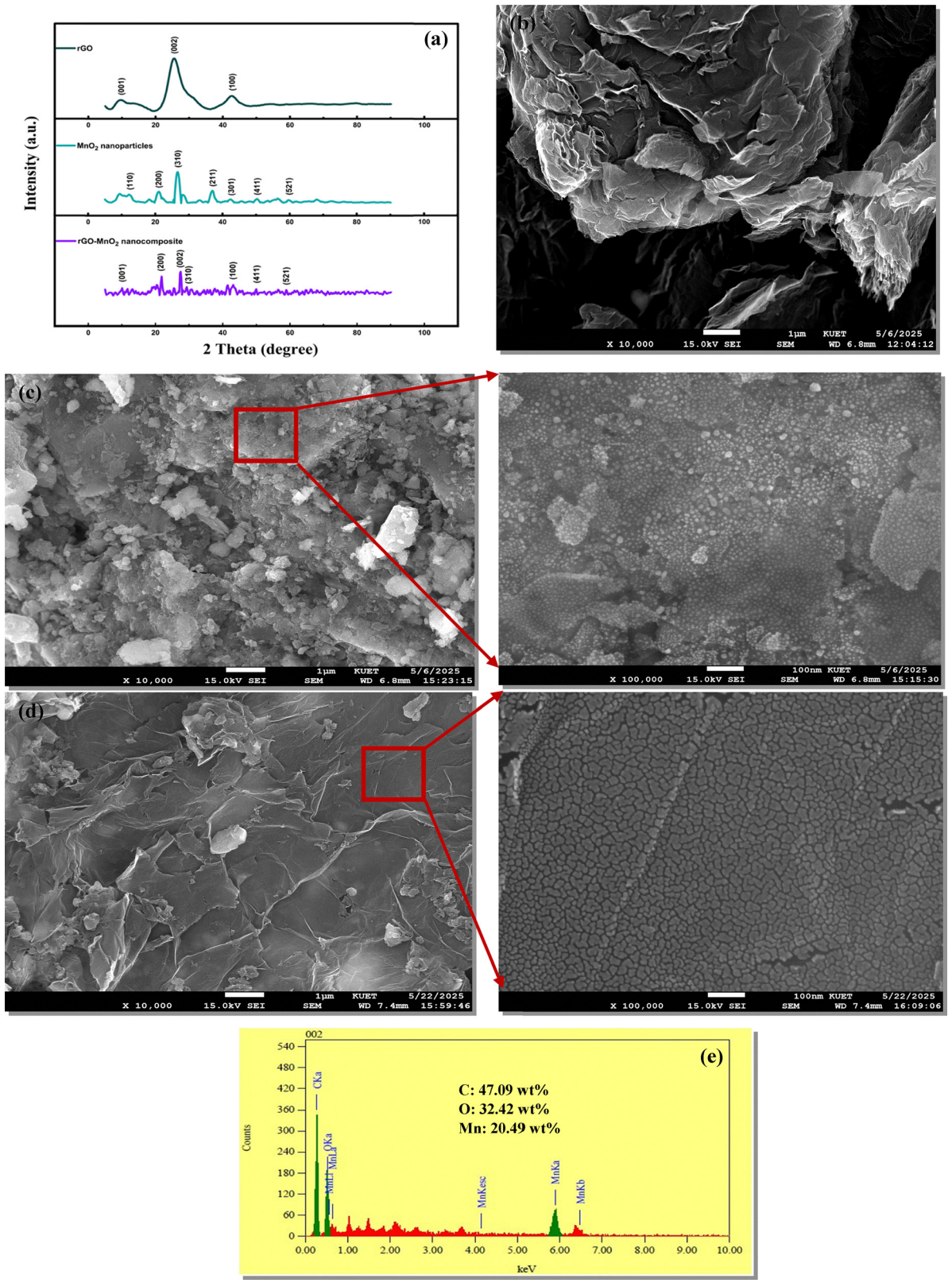

Fig. 2 (a) XRD plots of rGO, MnO_2 nanoparticles, and the rGO–MnO_2 nanocomposite. FESEM images of: (b) rGO, (c) MnO_2 nanoparticles, and the (d) rGO–MnO_2 nanocomposite, and (e) EDS results of the rGO–MnO_2 nanocomposite.

conduction pathways and a greater electrochemically active surface area. In the rGO–MnO_2 nanocomposite (Fig. 2d), MnO_2 nanoparticles were uniformly dispersed and tightly anchored onto the rGO sheets, forming a dense, interconnected nanoscale network. This architecture enables fast electron transport across the rGO framework allowing efficient diffusion of Hg^{2+} ions to reactive sites. As a result, the nanocomposite exhibits enhanced electrochemical reactivity and charge transfer kinetics. EDS analysis confirmed the elemental composition of the nanocomposite, with significant amounts of C, O, and Mn, further supporting the successful integration of both components.

The elemental analysis of rGO–MnO_2 nanocomposites was performed using EDS, as shown in Fig. 2(e). The EDS spectrum reveals distinct peaks corresponding to carbon (C), oxygen (O), and manganese (Mn), confirming the presence of rGO and MnO_2 in the composite. The quantitative analysis indicates that the composition consists of 47.09 wt% of C, 32.42 wt% of O, and 20.49 wt% of Mn, suggesting effective incorporation of MnO_2 into the rGO framework. These findings further support the effective synthesis of the rGO–MnO_2 nanocomposite with a homogenous distribution of elements.

3.2. Electrochemical characterization and optimization

CV was employed to determine the electroactive surface area of the GCE using a reputable redox probe solution that contained 5.0 mM $K_3[Fe(CN)_6]$ in 0.1 M KCl. For a reversible redox system at room temperature (25 °C), the Randles–Sevcik equation was used to calculate the electroactive surface area: $I_p = 2.69 \times 10^5 n^{3/2} A D^{1/2} C \nu^{1/2}$, where A is the electroactive surface area (cm^2), D is the diffusion coefficient of the redox species (7.6×10^{-6} cm^2 s^{-1}), C is the bulk concentration of the redox probe (5.0×10^{-6} mol cm^{-3}), ν is the scan rate (V s^{-1}), and I_p is the peak current (A). A diffusion-controlled electrochemical process was confirmed by the observation of linear dependence of the anodic peak current (I_p) on the square root of the scan rate ($\nu^{1/2}$). Based only on the anodic peak currents, the average electroactive area was determined to be about 0.227 cm^2, which is in good agreement with literature reports.[26] I_p *versus* $\nu^{1/2}$ is provided in Fig. S1 and the calculation of the active surface area of the GCE in Table S1.

The electrochemical behavior of the fabricated electrodes was evaluated by CV and EIS. Fig. 3(a and b) presents the CV and Nyquist plots acquired using a 5 mM $K_3Fe(CN)_6$ solution with 0.1 M KCl serving as the redox probe and supporting electrolyte, respectively. The measurements were performed on four different electrode configurations: bare GCE, MnO_2-modified GCE, rGO-modified GCE, and the rGO–MnO_2 nanocomposite-modified GCE. As shown in Fig. 3(a), the bare GCE exhibited the lowest redox current response, indicating limited electroactive surface area and sluggish electron-transfer kinetics. Modification with MnO_2 (MnO_2/GCE) resulted in a moderate increase in current due to the pseudocapacitive nature and surface activity of MnO_2, although its relatively low conductivity limited the enhancement. In contrast, rGO/GCE displayed the highest current response, about 0.23 mA, attributable to the excellent charge transport properties, large surface area, and rapid electron-transfer capability of rGO. The rGO–MnO_2 composite electrode demonstrated a current response (0.11 mA) higher than that of MnO_2/GCE (0.043 mA) and bare GCE (0.021 mA) but slightly lower than that of pure rGO, which can be attributed to the partial conductivity loss from MnO_2 incorporation. EIS was employed to evaluate the interfacial charge transfer characteristics of the electrode materials. The Nyquist plots in Fig. 3(b) of the bare GCE electrode showed the largest semicircular arc in the high-frequency region, reflecting a large charge transfer resistance (R_{ct}) in ohm and sluggish electron transfer kinetics. In comparison, the MnO_2/GCE and rGO/GCE displayed reduced R_{ct} values of 724 and 483 ohms, respectively. Whereas, the rGO–MnO_2/GCE electrode exhibited the lowest R_{ct} of 238 ohms. The observed reduction in resistance demonstrates the superior interfacial electron transfer performance of the nanocomposite-modified electrode. This enhancement arises from the complementary functions of MnO_2 and rGO, where MnO_2 provides numerous redox-active sites, while rGO contributes high electrical conductivity and provides a larger electroactive surface area.[17] The circuit model used to fit the EIS spectra, as shown in the inset of Fig. 3(b), consists of solution resistance (R_s), two resistances in parallel with constant phase element (CPE), where one is the film resistance (R_1) and the other is the charge transfer resistance (R_2), and a Warburg element (W) that accounts for ion diffusion at low frequencies. The more vertical Warburg tail observed for rGO–MnO_2/GCE in the low-frequency domain further indicates enhanced ion diffusion, facilitated by the porous and conductive nanostructure of the composite. Collectively, these results confirm that the rGO–MnO_2 nanocomposite exhibits excellent electrochemical performance, making it a promising material for high-sensitivity mercury detection.

To achieve optimal sensitivity for Hg^{2+} detection, the influence of both deposition potential and deposition time on stripping peak current was evaluated using SWASV with the rGO–MnO_2 modified GCE. Fig. 3(c) illustrates the influence of deposition time on the sensor's response. Deposition time is a critical parameter because it determines the duration available for Hg^{2+} ions to accumulate on the modified electrode surface before the stripping process. It was seen that the stripping peak current increases steadily with prolonged deposition time, indicating a greater accumulation of Hg^{2+} ions and thus a stronger electrochemical signal. The current reaches a plateau around 240 s, beyond which further extension of the deposition time does not yield significant improvements in peak current. This behavior implies that the electrode surface becomes saturated with Hg^{2+} ions, and further adsorption or reduction cannot occur beyond this point. Thus, 240 s was selected as the optimal deposition time. It provides effective duration for pre-concentration of Hg^{2+} ions without unnecessarily prolonging the analysis time, thus optimizing both sensitivity and efficiency.

Fig. 3(d) illustrates the influence of the deposition potential on stripping peak current during the electrochemical detection of Hg^{2+} ions. As the deposition potential shifts toward more

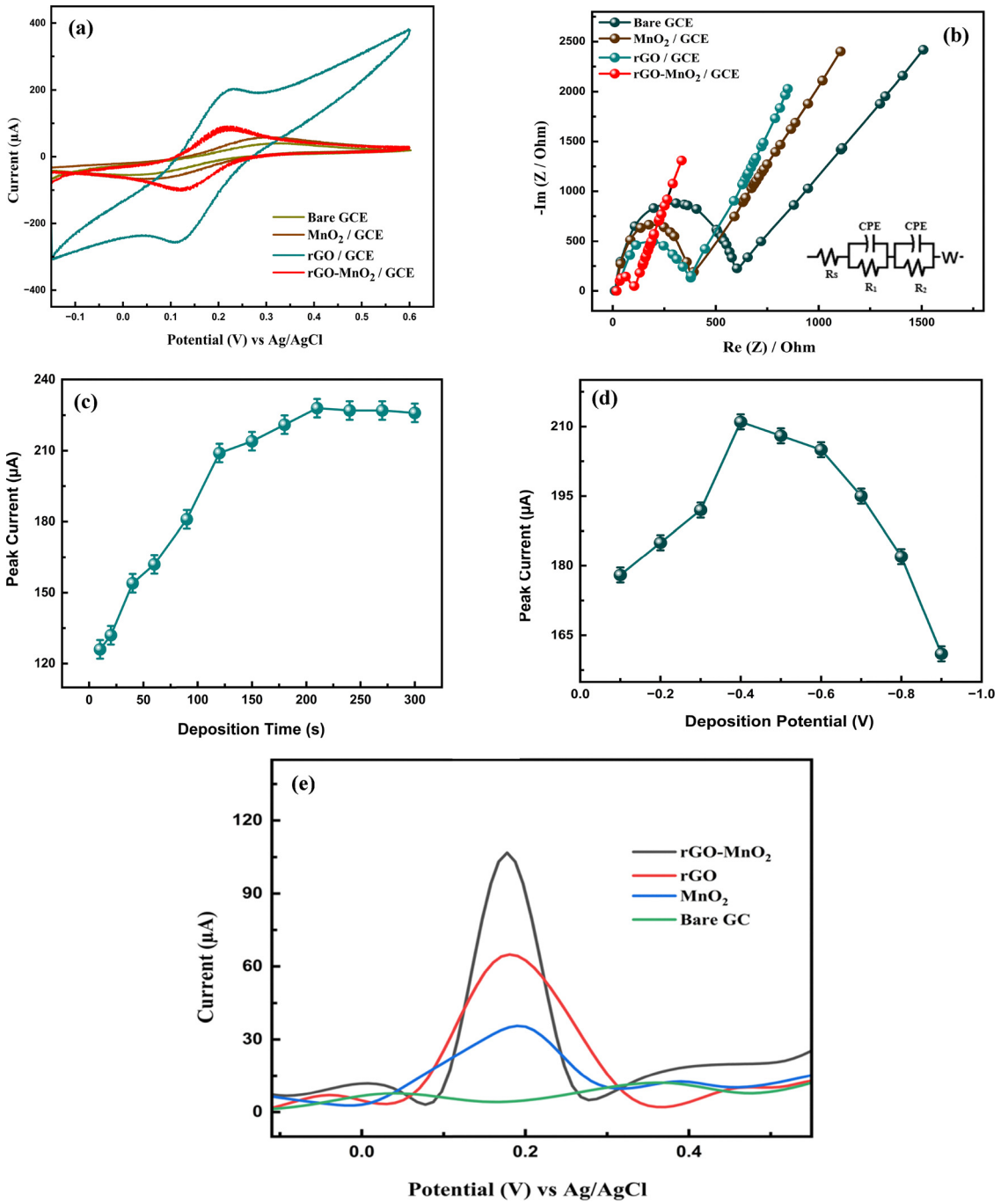

Fig. 3 (a) CV and (b) Nyquist plots for different electrodes in 5 mM $K_3Fe(CN)_6$ solution containing 0.1 M KCl. (i) bare GCE, (ii) MnO_2 modified GCE, (iii) rGO modified GCE, and (iv) rGO-MnO_2 modified GCE. The effect of (c) deposition potential and (d) deposition time on the stripping peak current for 5 μM Hg^{2+} at the rGO–MnO_2 nanocomposite modified GCE electrode. (e) SWASV responses for Hg^{2+} detection using bare, MnO_2, rGO, and rGO–MnO_2 modified GCE.

negative values, the current keeps increasing and reaches its maximum values near −0.4 V. This indicates that at this potential, Hg^{2+} ions are most effectively reduced to elemental mercury (Hg) on the electrode surface, allowing greater accumulation of Hg and enhancing oxidation current during the stripping step. When the potential exceeds −0.4 V in the negative direction, the peak current drops sharply. This decrease is likely due to unwanted side reactions, such as hydrogen evolution, which interfere with mercury deposition.[27] And also, too negative potentials may disrupt the stability or damage the electrode surface. Therefore, −0.4 V is taken as the most suitable deposition potential, providing efficient Hg^{2+} reduction while avoiding unwanted side reactions.

All electrochemical measurements were performed using 0.1 M KH_2PO_4 buffer solution with a pH of approximately 7.3. It represents the typical environmental water conditions and ensures stable electrochemical behavior of both the analyte and the electrode materials. This near-neutral pH provides several advantages for Hg^{2+} detection. At this pH, Hg^{2+} ions remain stable in solution and do not readily form insoluble hydroxide species. In addition, the electrochemical activity of MnO_2 and the oxygen-containing functional groups of rGO is preserved, while proton-coupled side reactions are minimized.[28] These conditions contribute to improved signal stability and reproducibility during stripping measurements.

Fig. 3(e) presents a comparative evaluation of the stripping peak currents obtained from four different electrode configurations, including the bare GCE, MnO_2, rGO, and rGO–MnO_2 modified GCE under optimized experimental conditions. Among the tested electrodes, the rGO–MnO_2 modified GCE exhibits the highest anodic stripping peak current, demonstrating its superior electrocatalytic activity and enhanced affinity toward Hg^{2+} ions. The synergistic effect of the rGO–MnO_2 nanocomposite material is responsible for this remarkable improvement in performance. The rGO component contributes high electrical conductivity with the large electroactive surface area, while MnO_2 plays multiple critical roles in the sensing process by providing oxygen-rich adsorption sites, such as Mn–O and O^{2-} species, which exhibit a strong affinity toward Hg^{2+} ions and promote effective pre-concentration on the electrode surface.[29] In addition, MnO_2 functions as a redox-active mediator that facilitates Hg^{2+} adsorption and its subsequent electrochemical reduction, while preferential Hg–O coordination enhances the selectivity of the sensor toward Hg^{2+} over competing ions. When combined with rGO, MnO_2 forms a synergistic heterostructure in which rGO ensures rapid electron transfer and high electrical conductivity, whereas MnO_2 contributes strong Hg^{2+} binding capability.[29] The combination leads to improved electron transfer kinetics and more effective preconcentration of Hg^{2+} at the electrode interface. The rGO-only and MnO_2-only modified electrodes show intermediate peak currents, each outperforming the bare GCE. This confirms that while both materials individually contribute to enhanced sensing, their integration into a single nanocomposite yields a significantly amplified response due to mutual reinforcement of their electrochemical properties. Thus, the rGO–MnO_2 nanocomposites demonstrate the advantage of using single-component modifications and validate their suitability for high-sensitivity Hg^{2+} detection in aqueous systems.

3.3. Detection of Hg^{2+} using the rGO–MnO_2 nanocomposite

The rGO–MnO_2 modified GCE has been applied for the detection of Hg^{2+} ions in three different concentration ranges, such as 1 mM to 10 mM, 1 μM to 10 μM, and 1 nM to 10 nM. Fig. 4(a-c) presents the SWASV response of the rGO–MnO_2 modified GCE in the presence of Hg^{2+} ions. A clear oxidation peak is observed at 0.2 V for Hg^{2+}, and a noticeable increase in the oxidation peak current with increasing concentrations of Hg^{2+} is seen, indicating efficient binding of Hg^{2+} and faster electron transport at the rGO–MnO_2 modified electrode surface. The variation in peak width at different Hg^{2+} concentrations is a characteristic of anodic stripping voltammetry. Higher concentrations (μM to mM) result in increased surface coverage and a quasi-continuous mercury layer due to Hg^0 accumulation. Diffusion- and film-controlled stripping enables Hg^0 oxidation to occur more synchronously within a limited potential range. The result is sharper, more intense stripping peaks. Hg^0 deposits are minimal at ultra-low concentrations (nM range) during the accumulation step. The rGO–MnO_2 surface unevenly distributes reduced mercury across high-energy active sites, causing adsorption and nucleation-controlled stripping. Under these conditions, Hg^0 oxidation gradually occurs over a wider potential window, resulting in less distinct stripping peaks. The ASV literature notes this transition from adsorption-controlled to diffusion-controlled stripping with increasing concentration, which explains concentration-dependent peak broadening,[31,32]

The inset of Fig. 4(a–c) further illustrates the calibration behavior of the rGO–MnO_2 sensor across a wide dynamic range, demonstrating a strong linear correlation with the regression equation of $y = 6.81x + 2.23$ ($R^2 = 0.99253$) for the 0–10 nM range, $y = 146.27x + 10.01$ ($R^2 = 0.99294$) for the 1–10 μM range, and $y = 299.35x + 17.47$ ($R^2 = 0.98984$) for the 1–10 mM range. Instead of exhibiting a single linear response over several orders of magnitude, three distinct linear calibration regions were obtained within the ranges of 1–10 nM, 1–10 μM, and 1–10 mM, with excellent linearity ($R^2 > 0.98$). Consequently, calibration slopes obtained in one concentration regime cannot be directly extrapolated to other regimes. Such concentration-dependent multilinear calibration behavior has been widely reported in stripping voltammetric metal-ion sensors and is considered intrinsic to the technique.[31,32]

The increasing slope of the calibration plots across the three ranges – 6.81 μA nM^{-1}, 146.27 μA nM^{-1}, and 299.35 μA nM^{-1} – indicates enhanced current sensitivity at higher analyte concentrations. These results not only confirm the rGO–MnO_2 nanocomposite's capability for detecting ultra-trace levels of Hg^{2+} with excellent linearity and precision but also demonstrate its effectiveness in moderately and heavily contaminated water samples. The enhanced electrochemical signal results from the synergistic integration of rGO sheets and MnO_2 nanoparticles, where rGO contributes high conductivity and a large surface area for electron transport, and MnO_2 provides abundant redox-active sites for electrocatalytic Hg^{2+} adsorption and reduction. This synergistic effect results in a highly active and stable sensing surface, capable of reliable mercury detection in complex aqueous environments. The strong correlation coefficients across all concentration ranges further confirm the reproducibility and robustness of the rGO–MnO_2-modified GCE, indicating it as a promising platform for sensitive, quantitative, and field-deployable electrochemical sensing of mercury ions in water. The high R^2 value obtained demonstrates strong linearity and reproducibility of the sensor within the studied concentration range. These confirm that the rGO–MnO_2 nanocomposite serves as a dependable and effective platform for sensitive and

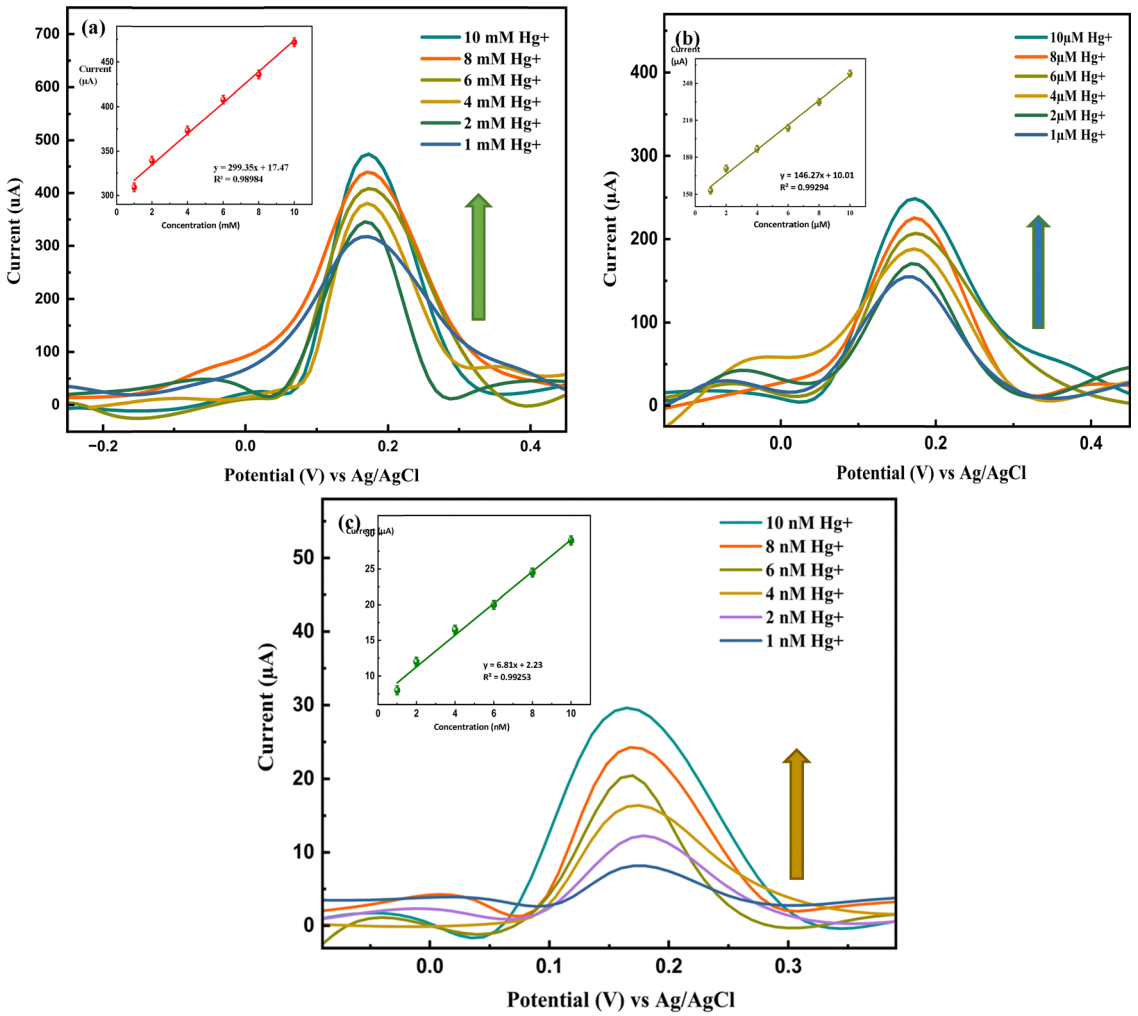

Fig. 4 SWASV responses of the rGO–MnO_2 modified GCE in 0.1 M KH_2PO_4 buffer (pH 7.3) containing different concentrations of Hg^{2+} in the range of (a) 1.0–10 mM, (b) 1.0–10 μM and (c) 1.0–10 nM. All data are reported as mean ± s.d. (n = 3).

quantitative detection of Hg^{2+} ions, highlighting its potential for electrochemical sensing applications.

To determine the detection and quantification limits, the limit of detection (LOD) and limit of quantification (LOQ) were evaluated using the blank signal standard deviation (σ) and the slope (S) of the calibration plot, following the well-established relations LOD = $3.3\sigma/S$ and LOQ = $10\sigma/S$. Here, σ reflects the baseline current fluctuations in the absence of Hg^{2+} ions, corresponding to the noise of the system. Based on the calibration slope for nM detection (S = 6.81 μA nM^{-1} and σ = 0.2 μA), the determined LOD and LOQ were 0.097 nM and 0.294 nM, respectively. These results indicate that the developed sensor is capable of providing high sensitivity with precision and capable of detecting ultra-trace concentrations of Hg^{2+} ions in aqueous solutions. Details of σ, LOD, and LOQ calculations for the rGO–MnO_2/GCE sensor are provided in Table S2.

3.4. Selectivity, repeatability, reproducibility, and stability

The selectivity of the rGO–MnO_2 modified GCE toward Hg^{2+} detection was systematically investigated by evaluating its electrochemical response in the presence of various potentially interfering metal ions, including Cu^{2+}, Fe^{3+}, Zn^{2+}, K^+, and Na^+, at a concentration of 10 μM. The results revealed that none of the tested interfering ions produced any significant current response or discernible stripping peaks. However, a sharp and well-defined stripping peak was observed for Hg^{2+}, approximately at 0.2 V, which is well separated from common organic oxidation.[32] This strong Hg–O coordination reduces susceptibility to chelators compared with weakly bound metal ions, thereby confirming the high degree of selectivity of rGO–MnO_2 towards Hg^{2+}. Chemically, the rGO–MnO_2 nanocomposite offers numerous oxygen-containing groups that serve as active binding sites for Hg^{2+} adsorption. These include hydroxyl (–OH), carbonyl (C═O), carboxyl (–COOH), and surface lattice oxygen (O^{2-}) groups from MnO_2. The affinity of Hg^{2+} ions and oxygen-rich functional groups facilitates the formation of stable Hg–O coordination bonds, thereby improving selective adsorption and efficient electron transfer.[33] FTIR spectra also confirm the chemical interactions between Hg^{2+} and the nanocomposite. The FTIR spectra of the rGO–MnO_2 nanocomposite before and after Hg^{2+} exposure displayed noticeable shifts and intensity changes in peak position and intensity.[34] The broad –OH

stretching vibration near ~3430 cm^{-1} showed a reduction in intensity and a slight red-shift, indicating hydrogen bonding or complex formation with Hg^{2+} ions.[35] Furthermore, the characteristic peaks of C=O and –COOH groups near ~1650 cm^{-1} were either weakened or shifted, supporting direct coordination with Hg^{2+} ions.[36] Additionally, the Mn–O stretching vibrations (~510–530 cm^{-1}) showed minor shifts, further supporting the interaction between Hg^{2+} ions and MnO_2 sites.[37] These spectral changes collectively confirm the chemical binding of Hg^{2+} to oxygenated functional groups on the rGO–MnO_2 surface, validating the proposed adsorption–reduction mechanism. Thus, the synergistic integration of redox-active MnO_2 and highly conductive rGO not only enhances sensitivity but also enables selective detection of Hg^{2+} ions in complex aqueous environments.

The sensor repeatability was evaluated by performing five consecutive measurements of the rGO–MnO_2 modified GCE in the presence of 10 μM Hg^{2+} concentration under the same conditions. The stripping peak currents obtained from these trials showed little variation, exhibiting a relative standard deviation (RSD) of just 1.03%. This low deviation confirms the high level of repeatability and signal consistency during successive applications of the same electrode. The RSD calculations for the repeatability test are provided in Table S3.

To examine the reproducibility of the fabrication process, three independently prepared rGO–MnO_2 modified GCEs were employed to detect 10 μM Hg^{2+} under identical conditions. Both electrodes yielded highly comparable stripping responses, with an RSD of 1.02%. These results affirm the reliability and uniformity of the electrode modification protocol, indicating that the method can consistently produce functionally equivalent sensors. Details of the reproducibility test including RSD calculations are provided in Table S4.

The long-term operational stability of the developed electrode was assessed over a 30 day period. Stripping voltammetry measurements were taken at three-day intervals while the electrodes were stored under ambient laboratory conditions. The sensor retained 96.23% of its initial response after 12 days and 92.34% even after 30 days, confirming outstanding long-term stability. The rGO–MnO_2 nanocomposite is chemically robust across neutral pH conditions and repeated redox cycling.[29] These results suggest that the rGO–MnO_2 nanocomposite layer remained physically and chemically intact, without noticeable degradation or detachment from the GCE surface. The durability is mainly due to the effective drop-casting and drying process, which preserved the mechanical robustness of the nanocomposite film. The percentage stability calculation is summarized in Table S5 (Fig. 5).

3.5. Sensing mechanism and morphological characteristics

The superior sensing ability of the rGO–MnO_2/GCE towards the Hg^{2+} detection attributed to the combined physical, chemical, and electrochemical properties of the nanocomposite. These properties enable a highly effective sensing mechanism that involves ion adsorption, redox reactions, and stripping analysis. Fig. 6 illustrates the redox reactions involved in the electrochemical detection of Hg^{2+} ions on the rGO–MnO_2 surface. The detection was based on SWASV, which involves a two-step electrochemical process. During the deposition (reduction) step, Hg^{2+} ions are electrochemically reduced to metallic Hg^0 at an optimized deposition potential of −0.40 V (*vs.* Ag/AgCl) for 240 s, enabling effective pre-concentration on the rGO–MnO_2-modified electrode surface. Subsequently, in the stripping (oxidation) step, the deposited Hg^0 is re-oxidized to Hg^{2+} during the anodic scan, producing a stripping current that is proportional to the Hg^{2+} concentration. All measurements were carried out under ambient conditions, and dissolved oxygen does not significantly influence the sensor response because the reduction of Hg^{2+} occurs at potentials more positive than oxygen reduction, while the stripping peak appears at approximately 0.2 V.[33] In addition, the negligible interference from other electroactive species during the oxidation step and the high selectivity of the sensor are attributed to the strong affinity of Hg^{2+} toward oxygen-containing functional groups on rGO and MnO_2, which effectively suppress competing redox processes.[30] The overall redox reactions occurring on the electrode surface can be described as follows:

$$\text{Reduction during accumulation: } Hg^{2+} + 2e^- \rightarrow Hg^0$$

$$\text{Oxidation during stripping: } Hg^0 \rightarrow Hg^{2+} + 2e^-$$

This redox cycle is made possible by the combined structural and chemical properties of the rGO–MnO_2 nanocomposite. The MnO_2 nanoparticles supply oxygen-rich functional groups (*e.g.*, O^{2-} and Mn–O), which have strong affinity for Hg^{2+} ions.[38] Concurrently, rGO contributes a highly conductive matrix with a large electroactive surface area, accelerating charge transfer during redox reactions. Hg^{2+} ions interact strongly with the oxygenated functional groups present on rGO, including hydroxyl (–OH), carboxyl (–COOH), and carbonyl (C=O) groups, through coordination and electrostatic interactions, facilitating strong chemical binding and pre-concentration of Hg^{2+} at the electrode surface,[39].[40] In addition, Hg^{2+} ions form Hg–O bonds with the lattice oxygen of MnO_2, reflecting the strong affinity of mercury toward oxygen-rich metal oxide surfaces. These interactions facilitate the formation of stable Hg–O–Mn bridging structures at the rGO–MnO_2 interface, which effectively anchor Hg^{2+} ions onto the electrode surface. The combined presence of multiple binding sites and strong interfacial interactions enhances Hg^{2+} adsorption, improves selectivity against competing ions, and promotes efficient electron transfer during the stripping process. Consequently, these synergistic interactions significantly contribute to the enhanced electrochemical response and overall sensing performance of the rGO–MnO_2-based Hg^{2+} sensor.

The interaction between Hg^{2+} and the rGO–MnO_2 nanocomposite was further confirmed by FTIR spectroscopy, as shown in Fig. 7. The FTIR spectra before and after Hg^{2+} exposure revealed characteristic changes in several functional group vibrations. The broad –OH stretching band around ~3430 cm^{-1} showed decreased intensity and a red-shift, indicating hydrogen

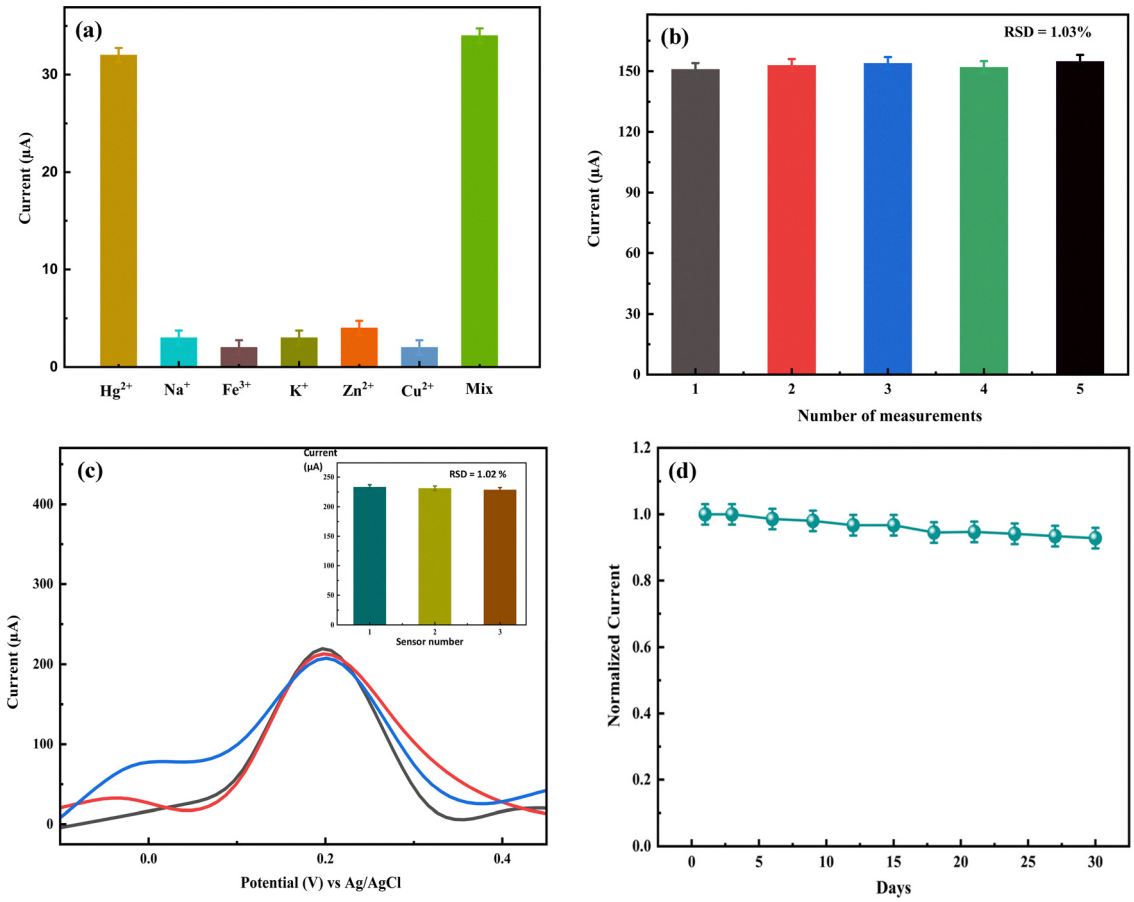

Fig. 5 (a) SWASV responses of the rGO–MnO_2 modified GCE for Hg^{2+} and other metal ions. The concentration of Hg^{2+} ions and the other interfering metal ions was 10 μM. (b) Repeatability analysis of the developed sensor for five replicated measurements. (c) Reproducibility of the developed sensor. Inset shows the histogram of peak current *versus* sensor number. (d) Stability of the rGO–MnO_2 modified GCE in response to 10 μM Hg^{2+} over 30 days using 0.1 M KH_2PO_4 buffer solution (pH 7.3).

bonding and complexation with Hg^{2+} ions.[35] The C═O stretching peak near ~1650 cm^{-1} was significantly weakened and slightly shifted, suggesting that carbonyl (C═O) and/or carboxyl (–COOH) groups coordinated directly with Hg^{2+} ions. In the Mn–O region (510–550 cm^{-1}), band shifts and the appearance of additional low-frequency components (~451 cm^{-1} and ~548 cm^{-1}) were consistent with the formation of Hg–O–Mn bridging structures.[36] These spectral shifts confirm the chemical bonding of Hg^{2+} to both rGO and MnO_2 functional

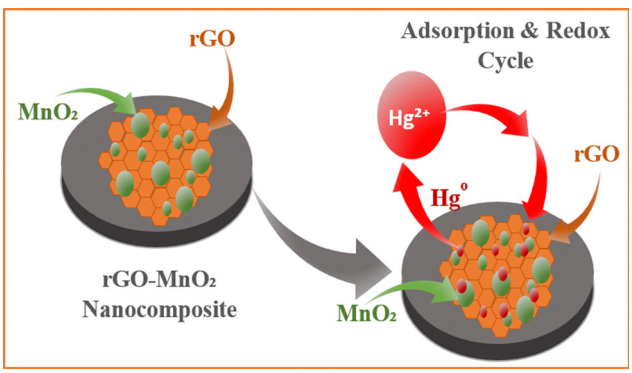

Fig. 6 Schematic of the rGO–MnO_2 nanocomposite modified electrochemical sensor for Hg^{2+} detection.

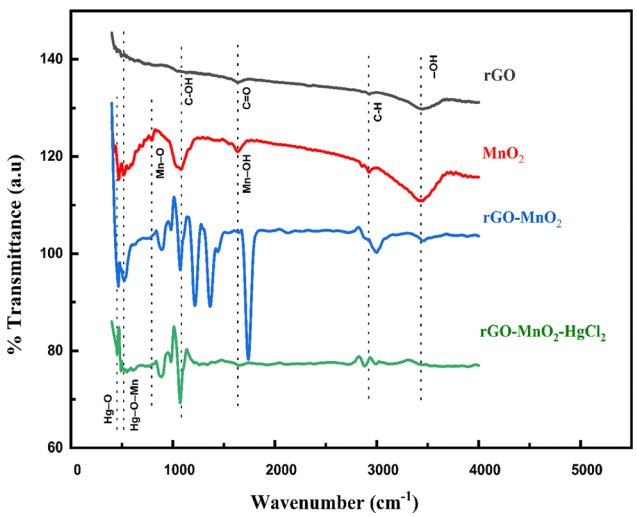

Fig. 7 FTIR spectra of rGO, MnO_2 nanoparticles, rGO–MnO_2 nanocomposite and rGO–MnO_2–$HgCl_2$ solution.

Table 1 Performance comparison of various electrochemical Hg^{2+} sensors

Sensor material/type	LOD	LDR	Method	Ref.
rGO–MnO_2 nanocomposite	0.097 nM	1 nM–10 mM	SWASV	This work
TBa modified GCE	2.5 $\times 10^{-15}$M	5 pM–100 nM	SWASV	43
ePdNPs@rGO/GCE	0.33 μM	1.0 nM–40 nM	LSV	44
MoS_2@MWCNT/GCE	2 nM	5 nM–500 nM	CV	45
N-doped rGO/MnO_2 nanocomposite	0.0414 nM	—	SWASV	46
Cu-MOFs@MnO_2-based ratiometric sensor	0.030 μM	—	DPSV	47

groups, validating a dual-mode adsorption mechanism involving surface complexation and redox-active coordination. The formation of stable Hg–O and Hg–O–Mn linkages contributes to the observed high selectivity and sensitivity of the sensor.[41,42] The rGO–MnO_2 nanocomposite functions through the combined roles of its constituents. MnO_2 provides high-affinity adsorption sites and actively participates in redox reactions, while rGO serves as a highly conductive platform for electron transfer and enables rapid signal response. The oxygen-containing groups in both materials form stable complexes with Hg^{2+} ions. The nanocomposite's structural features such as high surface area and porosity enhance ion access and reaction rates. These combined results demonstrate that the rGO–MnO_2 modified GCE operates through a redox-driven adsorption–desorption process with superior analytical performance in real-world water monitoring applications.

Table 1 provides a comprehensive performance comparison of various reported electrochemical sensors for the detection of Hg^{2+} ions. The rGO–MnO_2 nanocomposite demonstrates an impressive LOD of 0.097 nM and a wide linear detection range of 1 nM to 10 mM, which is superior to reported works.[35–38] In comparison, tetrabenzylammonium (TBa) modified GCE and TBa/AgNPs/GCE sensors, as reported in ref. 43, exhibit even lower detection limits of 2.5 $\times$ 10^{-15} M and 1.7 $\times$ 10^{-15} M, respectively. Both sensors utilize the SWASV technique and cover a linear range of 5 pM to 100 nM, making them highly effective for ultra-trace level detection of Hg^{2+} ions. However, the fabrication and stability of such ultra-sensitive platforms can be challenging in field applications.

The ePdNPs@rGO/GCE showed a detection limit of 0.33 μM and an LDR of 1.0 μM to 40 μM.[44] Although the LOD is higher, this system benefits from the catalytic activity of palladium nanoparticles, offering selective detection capabilities. MoS_2@MWCNT/GCE, reported in ref. 45, achieved an LOD of 2 nM and a linear range of 5 nM to 500 nM, making it moderately sensitive using general electrochemical techniques. This system leverages the synergistic effect of molybdenum disulfide and multi-walled carbon nanotubes. Among closely related systems, the N-doped rGO/MnO_2 nanocomposite sensor[44] achieved an ultralow detection limit of approximately 0.0414 nM due to enhanced electronic conductivity and strong Hg^{2+} affinity introduced by nitrogen dopants. While this sensor demonstrates a slightly lower LOD than the present work, it requires additional doping and synthesis complexity. In contrast, the rGO–MnO_2 nanocomposite developed in this study achieves comparable ultrasensitive detection performance using a simpler fabrication approach while maintaining excellent linearity, stability, and reproducibility. This highlights that effective Hg^{2+} sensing can be achieved through the intrinsic synergistic interaction between rGO and MnO_2, without the need for heteroatom doping or advanced surface engineering. Similarly, MnO_2-based MOF hybrid sensors utilizing rGO-like platforms have been reported for ratiometric detection of Hg^{2+}, achieving detection limits around 0.03 μM.[47] Although this system offers dual-analyte detection and strong selectivity through MOF-specific adsorption sites, their detection limits remain significantly higher than that obtained in the present work. Moreover, MOF-based platforms typically involve multi-step synthesis, stability concerns in aqueous media, and potential pore-blocking effects during prolonged use. In contrast, the rGO–MnO_2 nanocomposite sensor represented here offers a simpler architecture with superior sensitivity (0.097 nM), robust electrochemical stability, and reliable performance in aqueous matrices, making it more suitable for practical mercury monitoring applications.

Overall, the results demonstrate that the proposed rGO/MnO_2 sensor offers a highly competitive detection limit and an exceptionally wide linear detection range when compared with existing methods, reinforcing its potential applicability for practical environmental monitoring of Hg^{2+}contamination.

4. Conclusions

In summary, the rGO–MnO_2 nanocomposite has been successfully synthesized using a solution mixing process. The nanostructured rGO–MnO_2 has been utilized for fabricating the Hg^{2+} sensor, leveraging the synergistic effect of rGO and MnO_2. The structural and morphological properties of the rGO–MnO_2 nanocomposite have been confirmed by XRD, FESEM, and EDS. The CV and EIS revealed a significant reduction in R_{ct} and improved ion diffusion kinetics, indicating superior electrocatalytic activity. Optimal sensing conditions were established at a deposition potential of –0.4 V and an accumulation time of 240 s. Under optimized conditions, the sensor showed excellent sensitivity toward Hg^{2+} ions over a wide range of concentrations (nM, μM, and nM) with a low detection limit of 0.097 nM, surpassing WHO and EPA standards for Hg^{2+} in drinking water. The selectivity studies showed minimal interference from interfering metal ions such as Na^+, K^+, Cu^{2+}, Zn^{2+}, and Fe^{3+}. It exhibited high reproducibility and long-term stability, retaining over 92% of its initial response after 30 days of

storage. Overall, the rGO–MnO_2 nanocomposite modified sensor offers a stable platform with high sensitivity and selectivity for the trace level of Hg^{2+} detection. Its affordability, ease of use, and suitability for on-site analysis make it a promising tool for water quality monitoring, particularly in resource-limited settings. Furthermore, the proposed sensor requires minimal sample preparation, as water samples can be analyzed directly after buffering with 0.1 M KH_2PO_4 (pH 7.3) without complex pretreatment, enhancing feasibility for on-site applications. The Hg^{2+} stripping peak at approximately 0.2 V is well separated from the oxidation potentials of most common organic species, minimizing matrix interference. Furthermore, strong Hg–O coordination with oxygen-containing functional groups on the rGO–MnO_2 surface reduces susceptibility to complexing agents and competing ions, ensuring robust and reliable sensor performance in real water matrices. Although the present works demonstrates high sensitivity and a wide dynamic range for Hg^{2+} detection, further performance enhancement may be achieved through strategies such as heteroatom doping of rGO, surface functionalization, or hybridization with noble-metal nanoparticles. Such approaches are expected to further improve Hg^{2+} preconcentration efficiency and electron-transfer kinetics, thereby enabling even lower detection limits in future works.

Conflicts of interest

All authors declare that they have no conflict of interest.

Data availability

Data will be made available upon reasonable request.

Supplementary information is available. See DOI: https://doi.org/10.1039/d5ma01242b.

Acknowledgements

We sincerely acknowledge the Department of Electrical and Electronic Engineering at the Khulna University of Engineering & Technology (KUET), Khulna-9203, Bangladesh, for their continuous encouragement and research support. We are also grateful to the Department of Chemistry, KUET, for granting access to laboratory facilities and chemicals.

References

1 T. S. Munonde and P. N. Nomngongo, Nanocomposites for electrochemical sensors and their applications on the detection of trace metals in environmental water samples, *Sensors*, 2020, **21**(1), 131, DOI: 10.3390/s21010131.

2 M. Balali-Mood, K. Naseri, Z. Tahergorabi, M. R. Khazdair and M. Sadeghi, Toxic mechanisms of five heavy metals: mercury, lead, chromium, cadmium, and arsenic, *Front. Pharmacol.*, 2021, **12**, 643972, DOI: 10.3389/fphar.2021.643972.

3 M. T. Rahman, *et al.*, Metallic 1T Phase Tungsten Disulfide Microflowers for Trace Level Detection of Hg^{2+} Ions, *Adv. Sustain. Syst.*, 2020, **4**(9), 2000068, DOI: 10.1002/adsu.202000068.

4 R. Pant, N. Mathpal, R. Chauhan, A. Singh and A. Gupta, A review of mercury contamination in water and its impact on public health, in *Mercury Toxicity Mitigation: Sustainable Nexus Approach*, N. Kumar, ed., Earth and Environmental Sciences Library, Springer Nature Switzerland, Cham, 2024, pp. 93–115.

5 W. Ji, L. Li, Y. Zhang, X. Wang and Y. Ozaki, Recent advances in surface-enhanced Raman scattering-based sensors for the detection of inorganic ions: Sensing mechanism and beyond, *J. Raman Spectrosc.*, 2021, **52**(2), 468–481, DOI: 10.1002/jrs.5975.

6 T. Hu, Q. Lai, W. Fan, Y. Zhang and Z. Liu, Advances in portable heavy metal ion sensors, *Sensors*, 2023, **23**(8), 4125, DOI: 10.3390/s23084125.

7 R. Singh, R. Gupta, D. Bansal, R. Bhateria and M. Sharma, A review on recent trends and future developments in electrochemical sensing, *ACS Omega*, 2024, acsomega.3c08060, DOI: 10.1021/acsomega.3c08060.

8 N. T. Tonu and M. A. Yousuf, Low cost electrochemical sensor for simultaneous detection and estimation of dihydroxybenzene isomers port, *Electrochim. Acta*, 2022, **39**(6), 59–71, DOI: 10.4152/pea.2022400105.

9 F. Tan, L. Cong, N. M. Saucedo, J. Gao, X. Li and A. Mulchandani, An electrochemically reduced graphene oxide chemiresistive sensor for sensitive detection of Hg^{2+} ion in water samples, *J. Hazard. Mater.*, 2016, **320**, 226–233, DOI: 10.1016/j.jhazmat.2016.08.029.

10 L. Yang, L. Zhang, X. Jiao, Y. Qiu and W. Xu, The electrochemical performance of reduced graphene oxide prepared from different types of natural graphites, *RSC Adv.*, 2021, **11**(7), 4042–4052, DOI: 10.1039/D0RA09684A.

11 M. S. More, G. A. Bodkhe, F. Singh, M. Kim and M. D. Shirsat, Metal–organic framework-reduced graphene oxide (Zn-BDC@rGO) composite for selective discrimination among ammonia, carbon monoxide, and sulfur dioxide, *Appl. Phys. A: Mater. Sci. Process.*, 2023, **129**(12), 828, DOI: 10.1007/s00339-023-07103-0.

12 H. Zhang, *et al.*, Removal of aqueous Pb(II) by adsorption on Al_2O_3-pillared layered MnO_2, *Appl. Surf. Sci.*, 2017, **406**, 330–338, DOI: 10.1016/j.apsusc.2017.02.011.

13 D. Wang, *et al.*, MnO_2 nanoparticles anchored on carbon nanotubes with hybrid supercapacitor-battery behavior for ultrafast lithium storage, *Carbon*, 2018, **139**, 145–155, DOI: 10.1016/j.carbon.2018.06.046.

14 Y. Yang, *et al.*, Effects of synthesis temperature on ε-MnO_2 microstructures and performance: selective adsorption of heavy metals and the mechanism onto (100) facet compared with (001), *Environ. Pollut.*, 2022, **315**, 120218, DOI: 10.1016/j.envpol.2022.120218.

15 M. Lu, *et al.*, Evaluation of Fe_3O_4-MnO_2@RGO magnetic nanocomposite as an effective persulfate activator and metal adsorbent in aqueous solution, *Environ. Sci. Pollut.*

Res., 2023, **30**(17), 51125–51142, DOI: 10.1007/s11356-023-25911-y.

16 A. Pathak, M. Q. Khan, K. Ahmad, R. A. Khan, A. Chaudhary and T. H. Oh, Hydrothermally prepared α-MnO_2/N-rGO composite modified electrode for hydrazine sensing application, *J. Solid State Electrochem.*, 2025, **29**(2), 639–649, DOI: 10.1007/s10008-024-06080-5.

17 S. H. Mnyipika, T. S. Munonde and P. N. Nomngongo, MnO_2@Reduced graphene oxide nanocomposite-based electrochemical sensor for the simultaneous determination of trace Cd(II), Zn(II) and Cu(II) in water samples, *Membranes*, 2021, **11**(7), 517, DOI: 10.3390/membranes11070517.

18 M. T. Rahman, *et al.*, Graphene oxide–silver nanowire nanocomposites for enhanced sensing of Hg^{2+}, *ACS Appl. Nano Mater.*, 2019, **2**(8), 4842–4851, DOI: 10.1021/acsanm.9b00789.

19 S. L. Ting, S. J. Ee, A. Ananthanarayanan, K. C. Leong and P. Chen, Graphene quantum dots functionalized gold nanoparticles for sensitive electrochemical detection of heavy metal ions, *Electrochim. Acta*, 2015, **172**, 7–11, DOI: 10.1016/j.electacta.2015.01.026.

20 S. M. S. Al-Mufti, A. Almontasser and S. J. A. Rizvi, Single and double thermal reduction processes for synthesis reduced graphene oxide assisted by a muffle furnace: A facile robust synthesis and rapid approach to enhance electrical conductivity, *AIP Adv.*, 2022, **12**(12), 125306, DOI: 10.1063/5.0128803.

21 S. Khanmohammadi and M. Babazadeh, Synthesis of polythiophene/manganese dioxide nanocomposites by *in situ* core–shell polymerization method and study of their physical properties, *J. Nanostruct.*, 2018, **8**, 4, DOI: 10.22052/JNS.2018.04.006.

22 C. Liu, J. Wang, J. Tian and L. Xiang, Synthesis and surface characterization of γ-MnO_2 nanostructures, *J. Nanomater.*, 2013, **1**, 389634, DOI: 10.1155/2013/389634.

23 P. Rosaiah, *et al.*, Carbon based manganese oxide (MnO_2, MnO_2/MWCNT and MnO_2/rGO) composite electrodes for high-stability Li-ion batteries, *Carbon Lett.*, 2024, **34**(1), 215–225, DOI: 10.1007/s42823-023-00604-1.

24 Y. A. Tarek, R. Shakil, A. H. Reaz, C. K. Roy, H. R. Barai and S. H. Firoz, Wrinkled flower-like rGO intercalated with $Ni(OH)_2$ and MnO_2 as high-performing supercapacitor electrode, *ACS Omega*, 2022, **7**(23), 20145–20154, DOI: 10.1021/acsomega.2c01986.

25 S. Zhang, *et al.*, Wrinkled reduced graphene oxide nanosheets for highly sensitive and easy recoverable NH_3 gas detector, *RSC Adv.*, 2014, **4**(87), 46930–46933, DOI: 10.1039/C4RA08811E.

26 D. P. Rocha, C. W. Foster, R. A. A. Munoz, G. A. Buller, E. M. Keefe and C. E. Banks, Trace manganese detection *via* differential pulse cathodic stripping voltammetry using disposable electrodes: additively manufactured nanographite electrochemical sensing platforms, *Analyst*, 2020, **145**(9), 3424–3430, DOI: 10.1039/D0AN00018C.

27 J. A. Rodrigues, *et al.*, Increased sensitivity of anodic stripping voltammetry at the hanging mercury drop electrode by ultracathodic deposition, *Anal. Chim. Acta*, 2011, **701**(2), 152–156, DOI: 10.1016/j.aca.2011.05.031.

28 M. Saqib, *et al.*, Electrochemical detection of heavy metals using graphene-based sensors: advances, meta-analysis, toxicity, and sustainable development challenges, *Biosensors*, 2025, **15**(8), 505, DOI: 10.3390/bios15080505.

29 P. Wang, *et al.*, Manganese-based oxide electrocatalysts for the oxygen evolution reaction: a review, *J. Mater. Chem. A*, 2023, **11**(11), 5476–5494, DOI: 10.1039/D2TA09039B.

30 D. P. Shinde, *et al.*, Synergistic integration of δ-MnO_2/rGO composite electrode for enhanced electrochemical performance in supercapacitor applications, *Mater. Sci. Eng., B*, 2025, **322**, 118616, DOI: 10.1016/j.mseb.2025.118616.

31 C. Ariño, *et al.*, Electrochemical stripping analysis, *Nat. Rev. Methods Primer*, 2022, **2**(1), 62, DOI: 10.1038/s43586-022-00143-5.

32 A. J. Borrill, N. E. Reily and J. V. Macpherson, Addressing the practicalities of anodic stripping voltammetry for heavy metal detection: a tutorial review, *Analyst*, 2019, **144**(23), 6834–6849, DOI: 10.1039/C9AN01437C.

33 N. G. Yasri, A. K. Sundramoorthy, W.-J. Chang and S. Gunasekaran, Highly selective mercury detection at partially oxidized graphene/poly(3,4-ethylenedioxythiophene):poly(styrenesulfonate) nanocomposite film-modified electrode, *Front. Mater.*, 2014, **1**, DOI: 10.3389/fmats.2014.00033.

34 H. R. Ghenaatian, M. Shakourian-Fard and G. Kamath, Adsorption mechanism of toxic heavy metal ions on oxygen-passivated nanopores in graphene nanoflakes, *J. Mater. Sci.*, 2020, **55**(33), 15826–15844, DOI: 10.1007/s10853-020-05113-4.

35 F. Hamade, E. Radich and V. A. Davis, Microstructure and electrochemical properties of high performance graphene/manganese oxide hybrid electrodes, *RSC Adv.*, 2021, **11**(50), 31608–31620, DOI: 10.1039/D1RA05323J.

36 M. C. Terkhi, F. Taleb, P. Gossart, A. Semmoud and A. Addou, Fourier transform infrared study of mercury interaction with carboxyl groups in humic acids, *J. Photochem. Photobiol. Chem.*, 2008, **198**(2–3), 205–214, DOI: 10.1016/j.jphotochem.2008.03.018.

37 X. Zhang, *et al.*, Promoting effect of the core–shell structure of MnO_2@TiO_2 nanorods on SO_2 resistance in Hg_0 removal process, *Catalysts*, 2020, **10**(1), 72, DOI: 10.3390/catal10010072.

38 R. A. Lockwood and K. Y. Chen, Adsorption of mercury(II) by hydrous manganese oxides, *Environ. Sci. Technol.*, 1973, **7**(11), 1028–1034, DOI: 10.1021/es60083a006.

39 T. Tene, *et al.*, Removal of mercury(II) from aqueous solution by partially reduced graphene oxide, *Sci. Rep.*, 2022, **12**(1), 6326, DOI: 10.1038/s41598-022-10259-z.

40 L. Diao, *et al.*, Interface-engineered 3D porous MoS_2–ReS_2 in-plane heterojunction as efficient hydrogen evolution reaction electrocatalysts, *J. Colloid Interface Sci.*, 2024, **661**, 957–965, DOI: 10.1016/j.jcis.2024.02.056.

41 H. Xu, *et al.*, Stabilization of mercury over Mn-based oxides: speciation and reactivity by temperature programmed desorption analysis, *J. Hazard. Mater.*, 2017, **321**, 745–752, DOI: 10.1016/j.jhazmat.2016.09.030.

42 H. Liu, L. Ma, C. Ma, J. Du, M. Wang and K. Wang, Quencher-free fluorescence method for the detection of mercury(II) based on polymerase-aided photoinduced electron transfer strategy, *Sensors*, 2016, **16**(11), 1945, DOI: 10.3390/s16111945.

43 A. Manzoor, T. Kokab, A. Nawab, A. Shah, H. M. Siddiqi and A. Iqbal, Electrochemical detection of mercuric(II) ions in aqueous media using glassy carbon electrode modified with synthesized tribenzamides and silver nanoparticles, *RSC Adv.*, 2022, **12**(3), 1682–1693, DOI: 10.1039/D1RA08517D.

44 Z. Liu, M. Li, X. Zheng, X. Jia and Y. Guo, A highly selective mercury ion electrochemical detection based on the enhancement of oxidase-like activity by mercury on electrodeposited palladium nanoparticles@reduced graphene oxide, *New J. Chem.*, 2025, **49**(1), 28–37, DOI: 10.1039/D4NJ04023F.

45 J. Mishra, *et al.*, MoS_2@MWCNT modified glassy carbon electrode for electrochemical mercury(II) ion sensors, *J. Mater. Chem. C*, 2024, **12**(46), 18746–18756, DOI: 10.1039/D4TC02502D.

46 G.-L. Wen, *et al.*, N-doped reduced graphene oxide/MnO_2 nanocomposite for electrochemical detection of Hg^{2+} by square wave stripping voltammetry, *Electrochim. Acta*, 2018, **291**, 95–102, DOI: 10.1016/j.electacta.2018.08.121.

47 J. Liu, *et al.*, A Cu-MOFs@MnO_2 nanocomposite-based ratiometric electrochemical sensor for simultaneous detection of Pb^{2+} and Hg^{2+}, *Microchem. J.*, 2026, **221**, 116742, DOI: 10.1016/j.microc.2025.116742.